Eur. Phys. J. C 55, 285–292 (2008)
DOI 10.1140/epjc/s10052-008-0588-4

THE EUROPEAN PHYSICAL JOURNAL C

Regular Article – Theoretical Physics

Wilson line correlator in the MV model: relating the glasma to deep inelastic scattering

T. Lappi[a]

Institut de Physique Théorique, Bât. 774, CEA/DSM/Saclay, 91191 Gif-sur-Yvette Cedex, France

Received: 9 January 2008 / Revised version: 18 February 2008 /
Published online: 24 April 2008 –

Abstract. In the color glass condensate framework the saturation scale measured in deep inelastic scattering of high energy hadrons and nuclei can be determined from the correlator of Wilson lines in the hadron wavefunction. These same Wilson lines give the initial condition of the classical field computation of the initial gluon multiplicity and energy density in a heavy ion collision. In this paper the Wilson line correlator in both adjoint and fundamental representations is computed using exactly the same numerical procedure as has been used to calculate gluon production in a heavy ion collision. In particular the discretization of the longitudinal coordinate has a large numerical effect on the relation between the color charge density parameter $g^2\mu$ and the saturation scale Q_s. Our result for this relation is $Q_\mathrm{s} \approx 0.6 g^2\mu$, which results in the classical Yang–Mills value for the "gluon liberation coefficient" $c \approx 1.1$.

PACS. 24.85.+p; 25.75.-q; 13.60.Hb

1 Introduction

A useful description of the hadron or nucleus wavefunction at high energy is to view the small x degrees of freedom as classical color fields radiated by classical static color sources formed by the large x degrees of freedom [1–3]. This description, known as the color glass condensate (for reviews see e.g. [4, 5]), provides a common framework for understanding both small x deep inelastic scattering (DIS) and the initial stages of relativistic heavy ion collisions, both of which can be understood in terms of Wilson lines of the classical color field. The cross section for small x DIS can be expressed in terms of the correlator of two Wilson lines in the fundamental representation (i.e. the dipole cross section), and the initial condition for the classical fields that dominate the first fraction of a fermi of a heavy ion collision is determined by these same Wilson lines. The inverse of the correlation length of these Wilson lines is known as the *saturation scale* Q_s. The dipole cross section can be determined from the dipole model fits to DIS data on protons [6–10] and nuclei [11, 12] or extensions from the proton to the nucleus using a parametrization of the nuclear geometry [10, 13–17]. On the other hand there is a large body of both analytical [18–24] and numerical classical Yang–Mills (CYM) [25–33] computations of the "glasma" [34] fields in the initial stages of relativistic heavy ion collisions.

The aim of this paper is to relate the parameters of these two types of applications of color glass condensate ideas to each other more precisely. This is done by computing the Wilson line correlator in the McLerran–Venugopalan (MV) model [1–3], using exactly the same numerical method as has been used to compute the initial transverse energy and multiplicity in a heavy ion collision. By doing this we can relate the saturation scale Q_s, whose numerical value can be determined from fits to DIS data, to the color charge density $g^2\mu$, which determines the initial conditions for a heavy ion collision. The calculation relating these two parameters has been done analytically by several authors [35–41]. The procedure used to construct the MV model Wilson lines in this paper is the same as used in the numerical computations of the glasma fields and differs from these analytical computations in two ways. Firstly, as noted also in [42], the analytical computation is done by spreading out the color source in rapidity, while in the numerical computations this has not been done. We shall see that this introduces a difference of a factor of 2 in the actual numerical relation between Q_s and $g^2\mu$. Secondly the analytical result for the relation between Q_s and $g^2\mu$ depends logarithmically on the infrared cutoff that must be used in an intermediate stage of the computation, whereas in most of the numerical work the only such cutoff has been the size of the system. We shall also discuss the uncertainty arising from the non-Gaussian functional form of the Wilson line correlator and argue that it introduces an additional ambiguity at the 10% level. While the uncertainty from these aspects is parametrically unimportant (a constant or a logarithm), they must still be better understood in order to increase the predictive power of the calculations.

[a] e-mail: tuomas.lappi@cea.fr

The logic of this paper is that, instead of treating the color charge density $g^2\mu$ in the "glasma" calculations as a free phenomenological parameter, one should be able to relate it exactly, even the constant under the logarithm, to the saturation scale Q_s measured in DIS experiments. When DIS measurements are used to determine the value of the saturation scale, choosing what treatment of the rapidity direction to use in the MV model is mostly a matter of convenience as long as the value of $g^2\mu$ used is consistent with this chosen implementation. Let us note that our concern here is not as much the effects of the high energy evolution on the wavefunction, but the parametrization of the region $x \sim 0.01$ relevant for central rapidities at RHIC, which would be a reasonable initial condition for solving the BK or JIMWLK equation. The glasma field configurations obtained are the boost invariant fields that serve as the background for studying things like instabilities in the classical [43–45] field and higher order contributions to particle production [46–48].

We shall first introduce our notation for the Wilson line correlators in Sect. 2. Then our numerical results are presented in Sect. 3 and their implications for the interpretation of some of the earlier phenomenological work discussed in Sect. 4.

2 Wilson lines and glasma fields

Consider a high energy nucleus or a hadron moving along the x^+-axis. Its fast degrees of freedom can be considered as a classical color current:

$$J^+ = g\rho(\mathbf{x}_\mathrm{T}, x^-)\,, \tag{1}$$

which acts as a source to a classical color field representing the slower partons:

$$\left[D_\mu, F^{\mu\nu}\right] = J^\nu\,. \tag{2}$$

In the MV model the color charge density is taken to be a stochastic random variable with a Gaussian distribution.

In covariant gauge (2) can be solved as

$$A^+(x^-, \mathbf{x}_\mathrm{T}) = -\frac{g\rho(\mathbf{x}_\mathrm{T}, x^-)}{\boldsymbol{\nabla}^2_\mathrm{T}}\,. \tag{3}$$

The path ordered exponential of this field gives the Wilson line in the fundamental representation:

$$U(\mathbf{x}_\mathrm{T}) = P\mathrm{e}^{\mathrm{i}\int \mathrm{d}x^- A^+}\,. \tag{4}$$

It is this quantity that will concern us in the following.

The cross section for a virtual photon scattering off a high energy hadron or nucleus can be expressed in terms of the dipole cross section, which is determined by the correlator of two Wilson lines in the fundamental representation [5, 49]:

$$\tilde{C}(\mathbf{x}_\mathrm{T} - \mathbf{y}_\mathrm{T}) = \langle \mathrm{Tr}\, U^\dagger(\mathbf{x}_\mathrm{T}) U(\mathbf{y}_\mathrm{T})\rangle\,, \tag{5}$$

with the expectation value $\langle\,\cdot\,\rangle$ evaluated with the distribution of the sources.

The Wilson line in the adjoint representation is given by

$$U_{ab}(\mathbf{x}_\mathrm{T}) = 2\,\mathrm{Tr}\left[t^a U^\dagger(\mathbf{x}_\mathrm{T}) t^b U(\mathbf{x}_\mathrm{T})\right]. \tag{6}$$

The correlator of the adjoint representation Wilson lines

$$C(\mathbf{x}_\mathrm{T} - \mathbf{y}_\mathrm{T}) = \langle U_{ab}(\mathbf{x}_\mathrm{T}) U_{ab}(\mathbf{y}_\mathrm{T})\rangle \tag{7}$$

is related to the gluon distribution of a nucleus [35, 37, 50] (see [40, 51, 52] for a discussion on the intricacies of defining a gluon distribution in this case). With some algebra this adjoint representation correlator can be related to a higher correlator of fundamental representation Wilson lines:

$$C(\mathbf{x}_\mathrm{T} - \mathbf{y}_\mathrm{T}) = \left\langle |\,\mathrm{Tr}[U^\dagger(\mathbf{x}_\mathrm{T}) U(\mathbf{y}_\mathrm{T})]|^2 - 1\right\rangle, \tag{8}$$

which is the form we shall use to evaluate it numerically.

The initial conditions for the glasma fields are determined by the pure gauge fields (in light cone gauge) of the two colliding nuclei [18, 20]. In terms of the Wilson line (4) the pure gauge field of one nucleus is

$$A^i(\mathbf{x}_\mathrm{T}) = \frac{\mathrm{i}}{g} U(\mathbf{x}_\mathrm{T}) \partial_i U^\dagger(\mathbf{x}_\mathrm{T})\,, \tag{9}$$

and the initial conditions for the glasma fields are given by the sum and commutator of the pure gauge fields of the two nuclei. In the numerical computation of the glasma fields [25–31] there has been no longitudinal structure in the source, and the Wilson lines have been constructed simply as

$$U(\mathbf{x}_\mathrm{T}) = \exp\left\{-\mathrm{i}\frac{g\rho(\mathbf{x}_\mathrm{T})}{\boldsymbol{\nabla}^2_\mathrm{T}}\right\}, \tag{10}$$

with the transverse charge densities depending on a single parameter μ, independent of x^-:

$$\left\langle \rho^a(\mathbf{x}_\mathrm{T}) \rho^b(\mathbf{y}_\mathrm{T})\right\rangle = \delta^{ab}\delta^2(\mathbf{x}_\mathrm{T} - \mathbf{y}_\mathrm{T}) g^2\mu^2\,. \tag{11}$$

The analytical calculation [35–41] of the Wilson line correlator requires that, unlike the numerical procedure in [25–31], the source be extended in the x^- direction:

$$\begin{aligned}&\left\langle \rho^a(\mathbf{x}_\mathrm{T}, x^-) \rho^b(\mathbf{y}_\mathrm{T}, y^-)\right\rangle \\ &\quad = g^2\delta^{ab}\delta^2(\mathbf{x}_\mathrm{T} - \mathbf{y}_\mathrm{T})\delta(x^- - y^-)\mu^2(x^-)\,.\end{aligned} \tag{12}$$

With this longitudinal structure the Wilson line correlators can be computed analytically up to a logarithmic infrared cutoff that must be introduced in solving the Poisson equation (3). The result is

$$\begin{aligned}\tilde{C}(\mathbf{x}_\mathrm{T}) &\approx d_\mathrm{F} \mathrm{e}^{\frac{C_\mathrm{F}}{8\pi}\chi \mathbf{x}^2_\mathrm{T} \ln(m|\mathbf{x}_\mathrm{T}|)}\,,\\ C(\mathbf{x}_\mathrm{T}) &\approx d_\mathrm{A} \mathrm{e}^{\frac{C_\mathrm{A}}{8\pi}\chi \mathbf{x}^2_\mathrm{T} \ln(m|\mathbf{x}_\mathrm{T}|)}\,,\end{aligned} \tag{13}$$

with

$$\chi = g^4 \int \mathrm{d}x^- \mu^2(x^-)\,. \tag{14}$$

The dimensions and Casimir operators of the two representations in (13) are $d_{\mathrm{A}} = N_c^2 - 1$, $d_{\mathrm{F}} = N_c$, $C_{\mathrm{A}} = N_c$ and $C_{\mathrm{F}} = (N_c^2 - 1)/2N_c$. It could be argued that the cutoff m should be $\sim \Lambda_{\mathrm{QCD}}$. In any case, running coupling and confinement effects are not included in this treatment and the cutoff cannot be consistently defined within this calculation. When looking at length scales $|\mathbf{x}_{\mathrm{T}}| \ll 1/m$ results depend very weakly on this cutoff; in the lattice calculation it can be replaced by the finite size of the lattice. It would be very tempting to identify μ^2, the source strength of the delta function source, appearing in (11), with the integral over the spread distribution $\mu^2(x^-)$ of (14), but as we will see in the following, this correspondence is not exact.[1]

Note that the form (13) is compatible with the expectation that in the large N_c limit the four point function in (8) factorizes into a product of two point functions and

$$\lim_{N_c\to\infty} C(\mathbf{x}_{\mathrm{T}}) = \tilde{C}^2(\mathbf{x}_{\mathrm{T}})\,. \tag{15}$$

3 Numerical procedure and results

The Wilson lines used in the numerical calculation of the glasma fields [25–32] are SU(3) matrices defined on the sites of a 2 dimensional discrete lattice corresponding to the transverse plane. As in most of these calculations, we shall consider a square lattice with periodic boundary conditions and an average color charge density $g^2\mu^2$ that is constant throughout the plane. The Wilson lines are constructed as follows. On each lattice site $\mathbf{x}_{\mathrm{T}}$ one constructs random color charges with a local Gaussian distribution

$$\left\langle \rho_k^a(\mathbf{x}_{\mathrm{T}})\rho_l^b(\mathbf{y}_{\mathrm{T}})\right\rangle = \delta^{ab}\delta^{kl}\delta^2(\mathbf{x}_{\mathrm{T}} - \mathbf{y}_{\mathrm{T}})\frac{g^2\mu^2}{N_y}\,, \tag{16}$$

with the indices $k, l = 1, \ldots, N_y$ representing a discretized longitudinal coordinate. The numerical calculations so far have been done using $N_y = 1$, whereas the derivation of the analytical expression of the correlator, (13) are derived with an extended source, corresponding to the limit $N_y \to \infty$. Our normalization is chosen so that

$$\sum_{k,l}\left\langle \rho_k^a(\mathbf{x}_{\mathrm{T}})\rho_l^b(\mathbf{y}_{\mathrm{T}})\right\rangle = \delta^{ab}\delta^2(\mathbf{x}_{\mathrm{T}} - \mathbf{y}_{\mathrm{T}})g^2\mu^2\,. \tag{17}$$

The Wilson lines are then constructed from the sources (16) by solving a Poisson equation and exponentiating:

$$U(\mathbf{x}_{\mathrm{T}}) = \prod_{k=1}^{N_y}\exp\left\{-\mathrm{i}g\frac{\rho_k(\mathbf{x}_{\mathrm{T}})}{\boldsymbol{\nabla}_{\mathrm{T}}^2 + m^2}\right\}. \tag{18}$$

Here we have introduced an infrared regulator m for inverting the Laplace operator. This is the same regulator as the one appearing in the analytical expression (13). For large N_y the charge densities ρ_k in (16) become small, and the individual elements in the product (18) approach identity. This is precisely the procedure that leads in the $N_y \to \infty$ limit to the continuum path ordered exponential (4).

To summarize, our calculation depends on the following parameters.

- $g^2\mu$, determining the color charge density.
- N_y, the number of points in the discretization of the longitudinal (x^- or rapidity) direction.
- The infrared regulator m. When $m = 0$, as in most of the results presented, the Poisson equation is solved by leaving out the zero transverse momentum mode. This procedure corresponds to an infrared cutoff given by the size of the system.
- The lattice spacing a.
- The number of transverse lattice sites $N_\perp$, giving the size of the lattice $L = N_\perp a$.

Of the parameters a, $g^2\mu$ and m, only the dimensionless combinations $g^2\mu a$ and ma appear in the numerical calculation, and the continuum limit $a \to 0$ is taken by letting $N_\perp \to \infty$ so that $g^2\mu a \to 0$ and $g^2\mu L = g^2\mu a N_\perp$ remains constant. What we are looking at is a relatively infrared quantity and it thus should converge very well in the continuum limit. Based on the analytical calculation we may expect a logarithmic dependence of the saturation scale on $g^2\mu/m$ or, for $m = 0$, on $g^2\mu L$.

By Fourier transforming the Wilson lines we can then construct the momentum space correlators in the adjoint and fundamental representations, $C(\mathbf{k}_{\mathrm{T}})$ and $\tilde{C}(\mathbf{k}_{\mathrm{T}})$, respectively. These correlators, averaged over the polar angle, for different values of N_y are plotted in Fig. 1 as a function of

$$\tilde{k} = \frac{2}{a}\sqrt{\sum_{i=1}^{2}\sin^2(k_i a/2)}\,. \tag{19}$$

For small momenta the correlators look like Gaussians, which is the form used in the "GBW" fit of DIS data in [6–8]. For large momenta there is a power law tail $1/\mathbf{k}_{\mathrm{T}}^4$ that differs from the original GBW fits but resembles more closely the form required to match smoothly to DGLAP evolution for large Q^2 [53].

We define the numerically measured saturation scales as follows. The scale Q_{s} is determined by the adjoint representation Wilson line correlator as the momentum $\tilde{k}_{\max}$ corresponding to the maximum of $\tilde{k}^2 C(\mathbf{k}_{\mathrm{T}})$. This normalization in terms of the adjoint representation corresponds to that of [37, 50]. Similarly, from the maximum of the fundamental representation correlator $\tilde{k}^2\tilde{C}(\mathbf{k}_{\mathrm{T}})$ we define the fundamental representation saturation scale $\tilde{Q}_{\mathrm{s}}$ as $\tilde{Q}_{\mathrm{s}}^2 = \tilde{k}_{\max}^2$. Our definition of the saturation scale is not sensitive to the exact shape of the correlator for very large or small transverse momenta, and for a Gaussian correlator it reproduces the GBW saturation scale as $1/R_0^2 = \tilde{Q}_{\mathrm{s}}^2$. The saturation scale is expected to scale according to the Casimir operator of the representation, meaning $\tilde{Q}_{\mathrm{s}}^2 \approx \frac{C_{\mathrm{F}}}{C_{\mathrm{A}}}Q_{\mathrm{s}}^2$. In the plots (Figs. 2–4 and 6) we shall rescale

[1] It is relatively easy to see that the identification of $\int \mathrm{d}x^-\mu^2(\mathbf{x}_{\mathrm{T}}, x^-)$ with $\mu^2(\mathbf{x}_{\mathrm{T}})$ of (11) would be exact in the abelian case or in the large N_c limit in which the terms resulting from the noncommutative nature of ρ are suppressed.

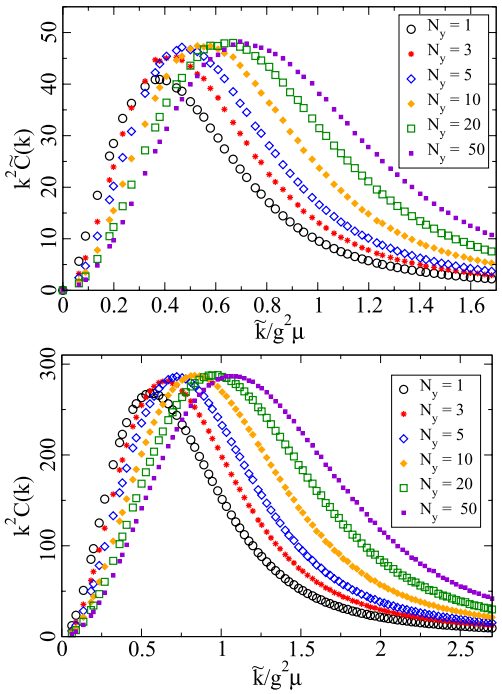

Fig. 1. The Wilson line correlator for $g^2\mu L = 100$ and different values of N_y. *Above*: fundamental representation $\tilde{k}^2\tilde{C}(\tilde{k})$, *below*: adjoint representation $\tilde{k}^2 C(\tilde{k})$

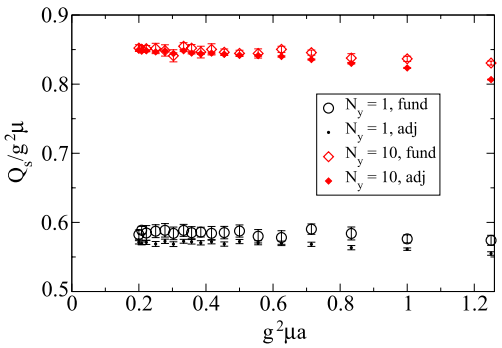

Fig. 2. The lattice spacing dependence of the saturation scales Q_s and $\sqrt{\frac{C_\mathrm{A}}{C_\mathrm{F}}}\tilde{Q}_\mathrm{s}$ for $g^2\mu L = 100$ and different N_y. The continuum limit is the $g^2\mu a = 0$ axis on the *left*

$\tilde{Q}_\mathrm{s}$ by this color factor to make the validity of this scaling clearer.

We first check the lattice spacing dependence of our result. Figure 2 shows that, as expected, the ratio $Q_\mathrm{s}/g^2\mu$ depends in fact so little on the lattice spacing that we will in the following not perform any continuum extrapolation for this quantity. The dependence of Q_s on the lattice size through the combination $g^2\mu L$ (without the additional infrared cutoff m) is shown in Fig. 3. The values used in the numerical computations of the glasma fields [25–33] correspond to $N_y = 1$ and $g^2\mu L \sim 100$ in Fig. 3, with $Q_\mathrm{s} \approx 0.57 g^2\mu$.

Figure 4 shows the dependence of $g^2\mu/Q_\mathrm{s}$ on the number of points used to discretize the longitudinal direction,

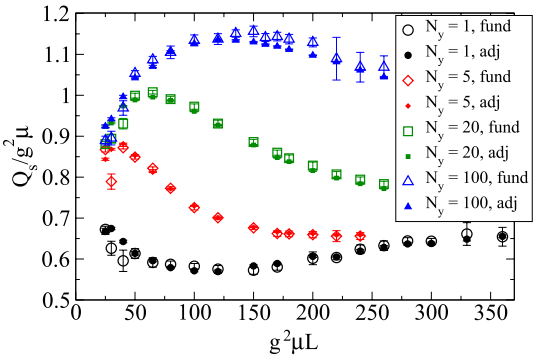

Fig. 3. The dependence of the adjoint and fundamental representation saturation scales Q_s and $\sqrt{\frac{C_\mathrm{A}}{C_\mathrm{F}}}\tilde{Q}_\mathrm{s}$ on $g^2\mu L$ for $g^2\mu a = 0.5$ and different N_y

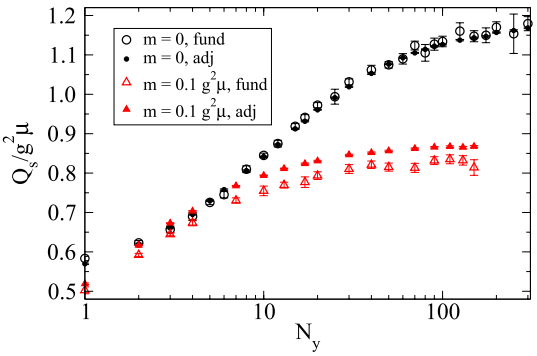

Fig. 4. Dependence on N_y of the saturation scales Q_s and $\sqrt{\frac{C_\mathrm{A}}{C_\mathrm{F}}}\tilde{Q}_\mathrm{s}$ for $g^2\mu L = 100$ and $g^2\mu a = 0.5$, shown for $m = 0$ and $m = 0.1 g^2\mu$

N_y. When $m = 0$, i.e. the infrared singularity is regulated only by leaving out the zero mode; there is approximately a difference of a factor of 2 between $Q_\mathrm{s} = 0.57 g^2\mu$ for $N_y = 1$ (the numerical CYM prescription) and $Q_\mathrm{s} \approx 1.15 g^2\mu$ for $N_y \to \infty$ (the analytical computation of the dipole cross section).[2] When the regulator $m = 0.1 g^2\mu$ is introduced the dependence on N_y is weaker, which can also be seen in Fig. 6. In Fig. 5 we show the same correlators as in Fig. 1 as a function of $\tilde{k}/Q_\mathrm{s}$ instead of $\tilde{k}/g^2\mu$. One sees that the correlator has a scaling form independent of N_y; from this only the $N_y = 1$ result deviates slightly. This suggests that, as argued in Sect. 1, once the appropriate relation between Q_s and $g^2\mu$ is used, and the physical results depend very little on N_y. Thus no significant change to the numerical CYM results should be expected if the calculations were repeated using a different treatment of the longitudinal coordinate in the source ρ.

Explicitly regulating the infrared behavior with a mass scale m makes it possible to compare the numerical result to the analytical one of (13). If one introduces an infrared scale m as in (10) and replaces $\ln(m|\mathbf{x}_\mathrm{T}|)$ with $-\ln(g^2\mu/m)$

[2] Because the initial energy density ϵ of the glasma is proportional to Q_s^4/g^2, this factor of 2 could be an explanation of the factor of 16 difference in $\epsilon/(g^2\mu)^4$ observed in [42].

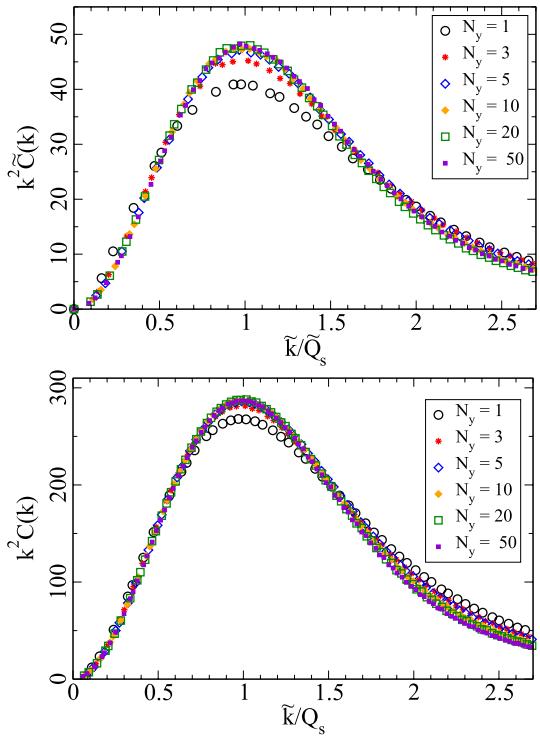

Fig. 5. The same fundamental representation Wilson line correlator as in Fig. 1 plotted as a function of the scaling variable $\tilde{k}/Q_s$. *Above*: fundamental representation $\tilde{k}^2\tilde{C}(\tilde{k})$ vs. $\tilde{k}/\tilde{Q}_s$, *below*: adjoint representation $\tilde{k}^2C(\tilde{k})$ vs. $\tilde{k}/Q_s$

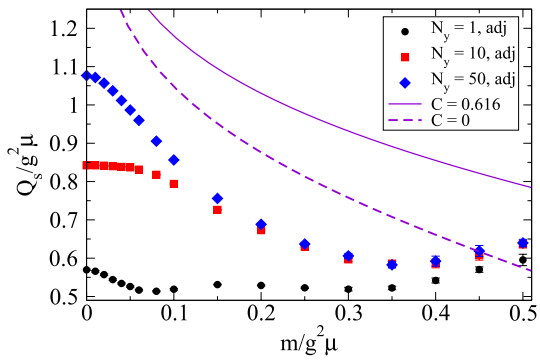

Fig. 6. Dependence on the regulator m of the saturation scale Q_s for $g^2\mu L = 100$. The *solid line* is the expected logarithmic dependence, (21) with the constant $C = 0.616$ and the *dashed one* with $C = 0$

in the coordinate space correlator, it becomes a Gaussian. Fourier transforming this, one obtains the estimate

$$\frac{Q_s^2}{(g^2\mu)^2} \approx \frac{C_A}{C_F}\frac{\tilde{Q}_s^2}{(g^2\mu)^2} \approx \frac{C_A}{2\pi}\left[\ln\frac{g^2\mu}{m} + \frac{1}{2} + \ln 2 - \gamma_E\right]. \tag{20}$$

Because of the replacement $|\mathbf{x}_T| \sim 1/g^2\mu$ there is still an uncertainty in the constant term. In Fig. 6 we plot the numerical result for $Q_s/g^2\mu$ as a function of $m/g^2\mu$ compared to the estimate

$$\frac{Q_s^2}{(g^2\mu)^2} = \frac{C_A}{2\pi}\left[\ln\frac{g^2\mu}{m} + C\right], \tag{21}$$

with values $C = \frac{1}{2} + \ln 2 - \gamma_E \approx 0.616$ and $C = 0$. In an intermediate range of $m/g^2\mu$ and for a large enough value of N_y (recall that the analytical result corresponds to $N_y \to \infty$) the behavior of $Q_s/g^2\mu$ is similar, but the normalization different.

Another common way to define the saturation scale is in terms of the coordinate space correlator $C(\mathbf{x}_T)$, because this is the object appearing in the calculation of most observables in DIS. Kowalski and Teaney [10] define the saturation scale $Q_{s,\mathrm{coord.}}$ from the condition that $C(\mathbf{x}_T) = d_A e^{-1/2}$ at $\mathbf{x}_T^2 = 2/Q_{s,\mathrm{coord.}}^2$. Note that the definition in [17], where the same IPsat model is used, differs slightly: $C(\mathbf{x}_T) = d_A e^{-1/4}$ at $\mathbf{x}_T^2 = 1/Q_{s,\mathrm{coord.}}^2$. This definition can also be used in the numerical CYM computation, most straightforwardly by Hankel transforming the correlator $C(|\mathbf{k}_T|)$ back into coordinate space. As shown in Fig. 7, using this definition is closer to the analytical estimate (21). The ratio of $Q_{s,\mathrm{coord.}}$ to our original definition of Q_s for different values of $g^2\mu L$ and N_y is plotted in Fig. 8.

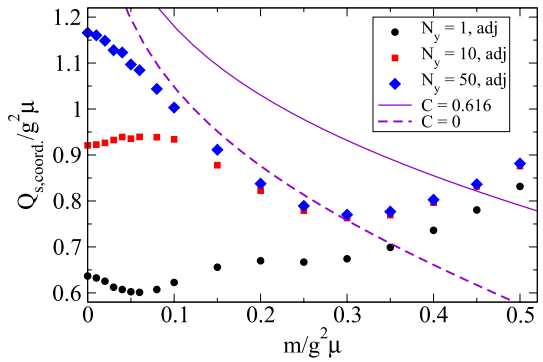

Fig. 7. Dependence on the regulator m of the coordinate space saturation scale $Q_{s,\mathrm{coord.}}$ for $g^2\mu L = 100$. The *solid line* is the expected logarithmic dependence, (21) with the constant $C = 0.616$ and the *dashed one* with $C = 0$

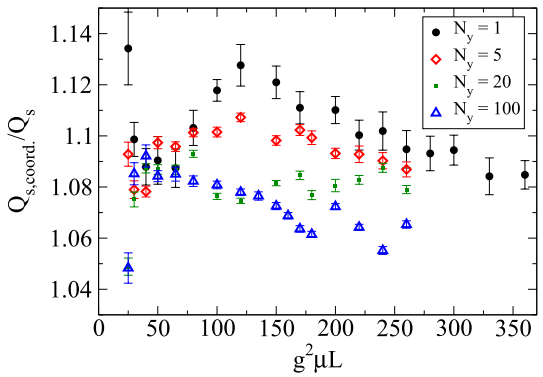

Fig. 8. The ratio of the two definitions of the saturation scale, the coordinate space definition ($Q_{s,\mathrm{coord.}}$) and the momentum space definition used in most of this paper (Q_s)

The difference between the two definitions is of the order of 10% with small variations. One must emphasize here that for an exactly Gaussian Wilson line correlator (the GBW form) the two definitions would be equal. They differ in the MV model, because the correlator is not Gaussian. Thus if one tries to determine $g^2\mu$ from a comparison to the experimental DIS data using GBW-type fits, which is one of the alternatives we consider in the next section, the ambiguity in the definition of Q_s leads to a 10% uncertainty in the value of $g^2\mu$.

4 Discussion

Let us finally use the results of the previous section for $Q_\mathrm{s}/g^2\mu$ and studies of DIS data to estimate the relevant value of $g^2\mu$ for RHIC physics. In deep inelastic scattering the variables x and Q^2 are precisely defined, and the saturation scale is a function of x, typically $Q_\mathrm{s}^2 \sim x^{-\lambda}$ with $\lambda \approx 0.3$. In the context of a heavy ion collision one is in fact, at a fixed energy and rapidity, summing up gluons produced at different transverse momenta and thus related to partons of different x in the nuclear wavefunction. The value of x at which to evaluate the saturation scale must therefore be some kind of effective x_eff, depending on the typical transverse momentum of the produced gluons,

$$x_\mathrm{eff} \sim \frac{\langle p_\mathrm{T}\rangle}{\sqrt{s}} \sim \frac{Q_\mathrm{s}}{\sqrt{s}}\,. \tag{22}$$

This introduces an additional uncertainty into our attempt to determine the color charge density based on the deep inelastic scattering data; by varying $\frac{1}{2}Q_\mathrm{s}/\sqrt{s} < x_\mathrm{eff} < 2Q_\mathrm{s}/\sqrt{s}$, we get an uncertainty of the order of 5%.

A simple starting point for our estimate is the GBW fit [6, 7], where the proton saturation scale (in the fundamental representation, which is convenient for DIS) is parametrized as

$$\tilde{Q}_\mathrm{s}^2 = \frac{1}{R_{0\,\mathrm{GBW}}^2} = Q_0^2 (x/x_0)^\lambda\,. \tag{23}$$

The result of the fit including charm quarks gives $\lambda = 0.277$ and $x_0 = 0.41 \times 10^{-4}$, with the one redundant parameter chosen as $Q_0 = 1\,\mathrm{GeV}$, while the fit without charm makes Q_s approximately 30% larger.

This result must then be extended to finite nuclei. Let us denote the nuclear modification of Q_s by $g(A) \equiv Q_{\mathrm{s}A}^2/Q_{\mathrm{s}p}^2$. The most straightforward theoretical expectation for the nuclear dependence would be $g(A) = A^{1/3}$. Freund et al. [11] perform a fit of the form $g(A) = A^\delta$ to the available nuclear DIS data and obtain $\delta = 1/4$. Taking into account modifications to the $A^{1/3}$ behavior of the nuclear radius leads Armesto et al. [12] to consider a fit of the form $g(A) \sim AR_p^2/R_A^2 = C[A/(A^{1/3} - 0.77A^{-1/3})^2]^{3\delta}$ with the result $\delta \approx 0.42$ and $C \approx 0.5$. Although for asymptotically large nuclei this would imply $g(A) \sim A^{0.42}$, for the physical case $A \lesssim 200$ the nuclear modification factor $g(A)$ obtained in [12] is actually less than $A^{1/4}$.

A more detailed description of the saturation scale in a nucleus can be obtained by the IPsat model [10, 16, 17]. HERA data and the DGLAP equations are used to parametrize the dipole cross section for a proton. Taking into account the fluctuations in the positions of the nucleons in the nucleus within a realistic nuclear geometry leads to a nuclear dipole cross section, from which also the saturation scale can be determined. As shown in [17] this picture leads to a good parameter free description of all the existing small x eA data. The result is a more realistic picture of an impact parameter dependent saturation scale also influenced by DGLAP evolution, where the nuclear geometry leads to a $g(A)$ that can roughly be understood as a $CA^{1/3}$-like dependence (with $C < 1$) enhanced by a logarithmic increase in A resulting from the DGLAP evolution. Because scattering off nuclei is less dominated by the dilute edge than in the proton, the typical Q_s (conveniently taken as corresponding to $b_\mathrm{med.}$, the median impact parameter in deep inelastic scattering) is closer to the maximal Q_s in the nucleus than in the proton. We shall use here for gold the value at $b_\mathrm{med.} \approx 4.2\,\mathrm{fm}$ and at $x = 0.005 \approx Q_\mathrm{s}/\sqrt{s}$.

Table 1 summarizes the estimated saturation scales for calculating the classical field at central rapidity in RHIC based on the different fits explained above. The table also shows the corresponding values of $g^2\mu = Q_\mathrm{s}/0.57$.

To set this result in perspective let us briefly recall the result of the numerical CYM computations. The energy and multiplicity per unit rapidity can be parametrized as

$$\frac{\mathrm{d}N}{\mathrm{d}\eta} = \frac{(g^2\mu)^2 \pi R_A^2}{g^2} f_N\,, \tag{24}$$

$$\frac{\mathrm{d}E_\mathrm{T}}{\mathrm{d}\eta} = \frac{(g^2\mu)^3 \pi R_A^2}{g^2} f_E\,, \tag{25}$$

where the numerical result is $f_E \approx 0.25$ and $f_N \approx 0.3$ (see in particular [29, 31] for the result). This leads to the estimate that, for central rapidity at RHIC, $1.3\,\mathrm{GeV} \lesssim g^2\mu \lesssim 2.1\,\mathrm{GeV}$. The lower limit comes from the requirement that the energy per unit rapidity has to be at least as large initially as it is finally. In boost invariant hydrodynamical ("Bjorken") flow, energy is transferred from central rapidities to the fragmentation region by $p\,\mathrm{d}V$ work, thus decreasing the energy at central rapidities, decreasing $\mathrm{d}E_\mathrm{T}/\mathrm{d}y$. It is very hard to imagine a process that would increase the energy at midrapidity, and thus the measured final transverse energy gives a lower limit to the initial energy and to $g^2\mu$. The upper limit follows from the requirement that the

Table 1. Results for the adjoint representation saturation scale from extrapolations of DIS data to RHIC central rapidity kinematics

	$Q_\mathrm{s}^\mathrm{RHIC}$ [GeV]	$g^2\mu$ [GeV]
Naive $A^{1/3}$	1.7	3.0
$A^{1/4}$ [11]	1.4	2.5
$CA^{4/9}$ [12]	1.3	2.2
IPsat, $\sim CA^{1/3}\ln A$ [17]	1.1	2.0

number of gluons in the initial state should be less than or equal to that of hadrons in the final state. In ideal hydrodynamical flow the two are related by entropy conservation, and nonequilibrium processes should increase entropy and consequently the multiplicity during the evolution, not decrease it. The measured hadron multiplicity thus gives an upper limit on the initial multiplicity and $g^2\mu$. Quark pair production [54, 55] or in general higher order processes would generically increase the initial multiplicity for a given $g^2\mu$ and thus decrease the upper limit for $g^2\mu$ below 2 GeV. The only overlap region between these estimates and the DIS based ones in Table 1 is around $g^2\mu \approx 2$ GeV. This is also close to the estimate, based on large x parton distribution functions, of [20], which was used in the CYM calculations of [26–28]. On the DIS side the value $g^2\mu \approx 2$ GeV agrees very well with the estimate using the IPsat model (see Table 1), but our present understanding of gluon production seems to be in contradiction with the other, more naive, DIS fits. On the ion–ion collision side, we have a large initial gluon multiplicity and rapid equilibration, leaving little room for higher order effects or additional gluon production during thermalization.

One feature of the numerical CYM calculations has been the apparent small fraction of the gluons in the initial nuclear wavefunction that are "freed" in the collision [50, 56]. The liberation coefficient c, introduced by Mueller [57], is defined by writing the produced gluon multiplicity as

$$\frac{\mathrm{d}N}{\mathrm{d}^2\mathbf{x}_\mathrm{T}\,\mathrm{d}y} = c\frac{C_\mathrm{F}Q_\mathrm{s}^2}{2\pi^2\alpha_\mathrm{s}}\,. \tag{26}$$

With (24) this leads to

$$c = \frac{\pi f_N}{2C_\mathrm{F}}\left(\frac{g^2\mu}{Q_\mathrm{s}}\right)^2. \tag{27}$$

The original expectation was that c should be of order unity. The analytical calculation by Kovchegov [50] gave the estimate $c \approx 2\ln 2 \approx 1.4$. Using (20) for the ratio $Q_\mathrm{s}/g^2\mu$ led to the interpretation [56, 58] that the CYM result would be $c \approx 0.5$. We now see that when $Q_\mathrm{s}/g^2\mu$ is computed consistently with the numerical calculation the resulting CYM value for the liberation coefficient is $c \approx 1.1$. We must emphasize that because c is defined in terms of the physical multiplicity and the physical correlation length Q_s, there is no large logarithmic or N_y uncertainty in the result $c \approx 1.1$. The non-Gaussianity of the MV model correlator, as seen in the differing coordinate and momentum space results for Q_s, does introduce an ambiguity at the 10% level.

Let us summarize the major sources of error in estimating the relevant value of the saturation scale for RHIC physics from the DIS data. We have already mentioned the questions of the Wilson line correlator not being exactly of the GBW form, the exact value of x to use and the considerable variance in the estimates of A dependence of Q_s. It is also possible that including a more realistic description of the transverse coordinate dependence of the saturation scale [10, 14, 17, 30, 59] in the CYM calculation will have an impact on the gluon multiplicity and energy in an ion–ion collision, modifying our previous discussion. The solution to the problems related to the shape of the correlator can be solved by using the actual solution of the BK or JIMWLK equations to understand both DIS data (as is done in [9]) and to calculate the glasma fields. Confirming the calculations like that of [17] relating the saturation descriptions of the proton and a nucleus will require more experimental input in the form of more data on small x DIS on nuclei. Finally and perhaps most importantly, the influence of quantum corrections and instabilities of small rapidity dependent fluctuations is not yet understood quantitatively.

Acknowledgements. The author would like to thank R. Venugopalan for numerous discussions and comments on the manuscript.

References

1. L.D. McLerran, R. Venugopalan, Phys. Rev. D **49**, 2233 (1994) [arXiv:hep-ph/9309289]
2. L.D. McLerran, R. Venugopalan, Phys. Rev. D **49**, 3352 (1994) [arXiv:hep-ph/9311205]
3. L.D. McLerran, R. Venugopalan, Phys. Rev. D **50**, 2225 (1994) [arXiv:hep-ph/9402335]
4. E. Iancu, R. Venugopalan, arXiv:hep-ph/0303204
5. H. Weigert, Prog. Part. Nucl. Phys. **55**, 461 (2005) [arXiv:hep-ph/0501087]
6. K. Golec-Biernat, M. Wusthoff, Phys. Rev. D **59**, 014017 (1999) [arXiv:hep-ph/9807513]
7. K. Golec-Biernat, M. Wusthoff, Phys. Rev. D **60**, 114023 (1999) [arXiv:hep-ph/9903358]
8. A.M. Stasto, K. Golec-Biernat, J. Kwiecinski, Phys. Rev. Lett. **86**, 596 (2001) [arXiv:hep-ph/0007192]
9. E. Iancu, K. Itakura, S. Munier, Phys. Lett. B **590**, 199 (2004) [arXiv:hep-ph/0310338]
10. H. Kowalski, D. Teaney, Phys. Rev. D **68**, 114005 (2003) [arXiv:hep-ph/0304189]
11. A. Freund, K. Rummukainen, H. Weigert, A. Schafer, Phys. Rev. Lett. **90**, 222002 (2003) [arXiv:hep-ph/0210139]
12. N. Armesto, C.A. Salgado, U.A. Wiedemann, Phys. Rev. Lett. **94**, 022002 (2005) [arXiv:hep-ph/0407018]
13. E. Levin, M. Lublinsky, Nucl. Phys. A **696**, 833 (2001) [arXiv:hep-ph/0104108]
14. E. Gotsman, E. Levin, M. Lublinsky, U. Maor, Eur. Phys. J. C **27**, 411 (2003) [arXiv:hep-ph/0209074]
15. E. Levin, M. Lublinsky, Nucl. Phys. A **712**, 95 (2002) [arXiv:hep-ph/0207374]
16. H. Kowalski, L. Motyka, G. Watt, Phys. Rev. D **74**, 074016 (2006) [arXiv:hep-ph/0606272]
17. H. Kowalski, T. Lappi, R. Venugopalan, Phys. Rev. Lett. **100**, 022303 (2008) [arXiv:0705.3047 [hep-ph]]
18. A. Kovner, L.D. McLerran, H. Weigert, Phys. Rev. D **52**, 3809 (1995) [arXiv:hep-ph/9505320]
19. A. Kovner, L.D. McLerran, H. Weigert, Phys. Rev. D **52**, 6231 (1995) [arXiv:hep-ph/9502289]
20. M. Gyulassy, L.D. McLerran, Phys. Rev. C **56**, 2219 (1997) [arXiv:nucl-th/9704034]
21. A. Dumitru, L.D. McLerran, Nucl. Phys. A **700**, 492 (2002) [arXiv:hep-ph/0105268]

22. Y.V. Kovchegov, D.H. Rischke, Phys. Rev. C **56**, 1084 (1997) [arXiv:hep-ph/9704201]
23. R.J. Fries, J.I. Kapusta, Y. Li, arXiv:nucl-th/0604054
24. K. Fukushima, Phys. Rev. C **76**, 021 902 (2007) [arXiv:0704.3625 [hep-ph]]
25. A. Krasnitz, R. Venugopalan, Nucl. Phys. B **557**, 237 (1999) [arXiv:hep-ph/9809433]
26. A. Krasnitz, R. Venugopalan, Phys. Rev. Lett. **84**, 4309 (2000) [arXiv:hep-ph/9909203]
27. A. Krasnitz, R. Venugopalan, Phys. Rev. Lett. **86**, 1717 (2001) [arXiv:hep-ph/0007108]
28. A. Krasnitz, Y. Nara, R. Venugopalan, Phys. Rev. Lett. **87**, 192 302 (2001) [arXiv:hep-ph/0108092]
29. A. Krasnitz, Y. Nara, R. Venugopalan, Nucl. Phys. A **727**, 427 (2003) [arXiv:hep-ph/0305112]
30. A. Krasnitz, Y. Nara, R. Venugopalan, Nucl. Phys. A **717**, 268 (2003) [arXiv:hep-ph/0209269]
31. T. Lappi, Phys. Rev. C **67**, 054 903 (2003) [arXiv:hep-ph/0303076]
32. T. Lappi, Phys. Rev. C **70**, 054 905 (2004) [arXiv:hep-ph/0409328]
33. T. Lappi, Phys. Lett. B **643**, 11 (2006) [arXiv:hep-ph/0606207]
34. T. Lappi, L. McLerran, Nucl. Phys. A **772**, 200 (2006) [arXiv:hep-ph/0602189]
35. J. Jalilian-Marian, A. Kovner, L.D. McLerran, H. Weigert, Phys. Rev. D **55**, 5414 (1997) [arXiv:hep-ph/9606337]
36. Y.V. Kovchegov, Phys. Rev. D **54**, 5463 (1996) [arXiv:hep-ph/9605446]
37. Y.V. Kovchegov, A.H. Mueller, Nucl. Phys. B **529**, 451 (1998) [arXiv:hep-ph/9802440]
38. L.D. McLerran, R. Venugopalan, Phys. Rev. D **59**, 094 002 (1999) [arXiv:hep-ph/9809427]
39. F. Gelis, A. Peshier, Nucl. Phys. A **697**, 879 (2002) [arXiv:hep-ph/0107142]
40. J.P. Blaizot, F. Gelis, R. Venugopalan, Nucl. Phys. A **743**, 13 (2004) [arXiv:hep-ph/0402256]
41. J.P. Blaizot, F. Gelis, R. Venugopalan, Nucl. Phys. A **743**, 57 (2004) [arXiv:hep-ph/0402257]
42. K. Fukushima, arXiv:0711.2364 [hep-ph]
43. P. Romatschke, R. Venugopalan, Phys. Rev. Lett. **96**, 062 302 (2006) [arXiv:hep-ph/0510121]
44. P. Romatschke, R. Venugopalan, Phys. Rev. D **74**, 045 011 (2006) [arXiv:hep-ph/0605045]
45. K. Fukushima, F. Gelis, L. McLerran, Nucl. Phys. A **786**, 107 (2007) [arXiv:hep-ph/0610416]
46. F. Gelis, R. Venugopalan, Nucl. Phys. A **776**, 135 (2006) [arXiv:hep-ph/0601209]
47. F. Gelis, R. Venugopalan, Nucl. Phys. A **779**, 177 (2006) [arXiv:hep-ph/0605246]
48. F. Gelis, T. Lappi, R. Venugopalan, Int. J. Mod. Phys. E **16**, 2595 (2007) [arXiv:0708.0047 [hep-ph]]
49. K. Rummukainen, H. Weigert, Nucl. Phys. A **739**, 183 (2004) [arXiv:hep-ph/0309306]
50. Y.V. Kovchegov, Nucl. Phys. A **692**, 557 (2001) [arXiv:hep-ph/0011252]
51. D. Kharzeev, Y.V. Kovchegov, K. Tuchin, Phys. Rev. D **68**, 094 013 (2003) [arXiv:hep-ph/0307037]
52. F. Gelis, A.M. Stasto, R. Venugopalan, arXiv:hep-ph/0605087
53. J. Bartels, K. Golec-Biernat, H. Kowalski, Phys. Rev. D **66**, 014 001 (2002) [arXiv:hep-ph/0203258]
54. F. Gelis, K. Kajantie, T. Lappi, Phys. Rev. C **71**, 024 904 (2005) [arXiv:hep-ph/0409058]
55. F. Gelis, K. Kajantie, T. Lappi, Phys. Rev. Lett. **96**, 032 304 (2006) [arXiv:hep-ph/0508229]
56. A.H. Mueller, Nucl. Phys. A **715**, 20 (2003) [arXiv:hep-ph/0208278]
57. A.H. Mueller, Nucl. Phys. B **572**, 227 (2000) [arXiv:hep-ph/9906322]
58. R. Baier, A.H. Mueller, D. Schiff, D.T. Son, Phys. Lett. B **539**, 46 (2002) [arXiv:hep-ph/0204211]
59. T. Lappi, R. Venugopalan, Phys. Rev. C **74**, 054 905 (2006) [arXiv:nucl-th/0609021]